Bidirectional reflectance distribution function of Spectralon white reflectance standard illuminated by incoherent unpolarized and plane-polarized light

Anak Bhandari,[1,*] Børge Hamre,[1] Øvynd Frette,[1] Lu Zhao,[1] Jakob J. Stamnes,[1] and Morten Kildemo[2]

[1]Department of Physics and Technology, University of Bergen, N-5007 Bergen, Norway

[2]Department of Physics, Norwegian University of Science and Technology, N-7491 Trondheim, Norway

*Corresponding author: Anak.Bhandari@ift.uib.no

Received 15 April 2011; accepted 19 April 2011;
posted 29 April 2011 (Doc. ID 145271); published 25 May 2011

A Lambert surface would appear equally bright from all observation directions regardless of the illumination direction. However, the reflection from a randomly scattering object generally has directional variation, which can be described in terms of the bidirectional reflectance distribution function (BRDF). We measured the BRDF of a Spectralon white reflectance standard for incoherent illumination at 405 and 680 nm with unpolarized and plane-polarized light from different directions of incidence. Our measurements show deviations of the BRDF for the Spectralon white reflectance standard from that of a Lambertian reflector that depend both on the angle of incidence and the polarization states of the incident light and detected light. The non-Lambertian reflection characteristics were found to increase more toward the direction of specular reflection as the angle of incidence gets larger.

OCIS codes: 120.5410, 120.5820, 290.1483, 290.5880.

1. Introduction

Spectralon white reflectance standards are the International Commission on Illumination (CIE)-recommended light diffusing surfaces that are commercially available from Labsphere Corporation [1]. They are made of thermoplastic materials, which are resin machined into flat, thermally stable, high-permittivity surfaces with porosity within the top layer (generally a few tenths of a millimeter thick) that randomizes the phase of the incident light—due to internal multiple reflections—to produce diffuse reflected light. Because of their stable optical properties over the ultraviolet–visible–near-infrared spectral region, Spectralon white reflectance standards are widely used as reference standards for the calibration of photometric instruments on the ground as well as on-board satellites. The same materials are also used to make integrating spheres, which are reflectance accessories [2] for the creation of diffuse light sources. In the visible spectral range, the hemispherical reflectance of the Spectralon white reflectance standard is claimed to be larger than 98% [3] with Lambertian characteristics.

As mentioned above, the surface of a Spectralon reflection standard is porous, implying that the diffusely reflected light, to a significant degree, may be due to internal multiple reflections beneath its surface. For that reason, a random-surface model may not be adequate for simulating the Spectralon bidirectional reflectance distribution function (BRDF). Instead, one might use a model similar to that presented recently [4] to simulate radiation transport in coupled atmosphere–snow–ice–ocean systems, in which case there are contributions to the diffuse

0003-6935/11/162431-12$15.00/0

reflected light from a possible snow layer on top of the ice, a rough ice surface, and randomly located particles (bubbles and brine pockets) within the ice. Such simulations, however, are beyond the scope of this paper.

For collimated incident light, Haner *et al.* [5] measured the hemispherical reflectance from Spectralon and found its average value equal to 0.971 ± 0.04 for the visible and near-infrared spectral regions. Such a nonabsorbing surface should reflect the incident light equally in all directions with radiance proportional to the irradiance of the incident light. Voss and Zhang [6] found the reflectance characteristics of Spectralon white reflectance standards to be nearly Lambertian only for illumination at normal incidence. Early *et al.* [7] found the BRDF of a Spectralon white reflectance standard to depend on the illumination and viewing directions, but their measurement results did not include polarization effects. Georgiev and Butler [8] studied aging effects on the Spectralon BRDF in the UV and visible spectral ranges. They used polarized incident light but reported measurements only of unpolarized scattered light.

Haner *et al.* [9] measured the BRDF of a Spectralon white reflectance standard for coherent, plane-polarized illumination at four different angles of incidence and concluded that the BRDF varied with the observation angle, the angle of incidence, and the polarization state of incident light. For illumination they used coherent laser light, which generates speckle [10,11] in the BRDF profile due to interference effects. In contrast, we used incoherent illumination to avoid speckle effects and did most measurements in a plane outside the plane of incidence. Also, we examined a Spectralon white reflectance standard (SRS-99-020) different from that investigated by Haner *et al.* [9] (position 1 of Spectralon test sample number 12969). The effects on the BRDF of using polarized light from a 75 W xenon lamp to illuminate a Spectralon white reflectance standard was investigated by Georgiev and Butler [12], who found the BRDF of the Spectralon white reflectance standard to strongly depend on the polarization state of the incident light.

When the incident light is polarized, the reflected radiance will generally be partially polarized to a degree that depends on the nature of the random scattering process caused by the surface roughness as well as by volume scattering events beneath the surface. As discussed by Germer [13], the scattering of polarized light from the Spectralon standard is likely to be due mainly to volume scattering events.

A. BRDF

The reflectance of an object is generally quantified in terms of its albedo, which is the fraction of the incident radiative energy reflected from it. The albedo is dimensionless, and it characterizes the total hemispherical reflectance, whereas the BRDF describes how the reflectance varies as a function of illumination direction, observation direction, wavelength, and polarization. The BRDF [sr^{-1}] as defined by Nicodemus [14] is the ratio of the reflected radiance $L[\mathrm{W\ \ m^{-2}\ \ sr^{-1}}]$ to the incident irradiance $E[\mathrm{W\ \ m^{-2}}]$. It is an intrinsic optical property that varies from one surface to another, and it may also vary with the position on a given surface.

Consider an angular beam of radiation of frequency ν that is incident on the surface of diffusely scattering object with radiance $L(\nu, \hat{\Omega}')$ [$\mathrm{W\ \ m^{-2}\ \ sr^{-1}}$] within a cone of solid angle $d\omega'$ around the direction of incidence defined by the unit vector $\hat{\Omega}'(\theta', \phi')$ as illustrated in Fig. 1, so that the irradiance $E(\nu, \hat{\Omega}')$ incident on the surface is given by $L(\nu, \hat{\Omega}') \cos\theta' d\omega'$ [$\mathrm{W\ \ m^{-2}}$]. We let $L(\nu, \hat{\Omega}', \hat{\Omega})$ be the radiance of the reflected light leaving the diffusely scattering object in the observation direction given by the unit vector $\hat{\Omega}(\theta, \phi)$, and we define the directional reflectance, or BRDF, as the ratio of the reflected radiance to the incident irradiance, i.e.,

$$\rho(\nu, \hat{\Omega}', \hat{\Omega}) = \frac{L(\nu, \hat{\Omega}', \hat{\Omega})}{E(\nu, \hat{\Omega}')} = \frac{L(\nu, \hat{\Omega}', \hat{\Omega})}{L(\nu, \hat{\Omega}') \cos\theta' d\omega'} [\mathrm{sr}^{-1}]. \quad (1)$$

Note that Eq. (1) gives the scalar definition of the BRDF, which is appropriate for unpolarized illumination and detection, and does not account for the polarization states of the incident and scattered light. Adding the contributions to the reflected radiance in the direction $\hat{\Omega}$ from beams incident on the diffusely scattering object in all directions $\hat{\Omega}'$, we obtain the reflected radiance

$$L(\nu, \hat{\Omega}) = \int_{2\pi} \mathrm{d}\omega' \cos\theta' \rho(\nu, \hat{\Omega}', \hat{\Omega}) L(\nu, \hat{\Omega}'), \quad (2)$$

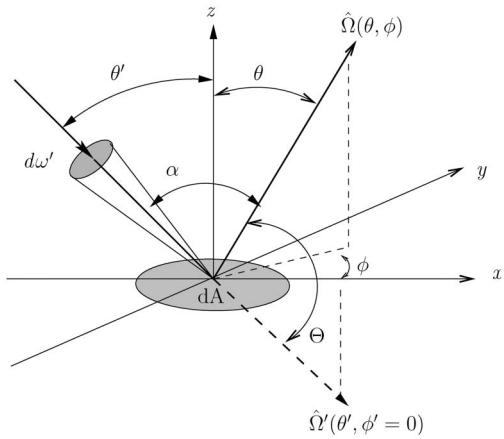

Fig. 1. Geometry and symbols for the definition of the BRDF. The normal to the surface area dA of a diffusely scattering object is taken to be along the z axis, and the incident beam along the unit vector $\hat{\Omega}'(\theta', \phi')$ is taken to lie in the x–z plane with azimuth angle $\phi' = 0°$. The observation direction is along the unit vector $\hat{\Omega}(\theta, \phi)$, and α is the backscattering angle, which is given by $\alpha = \pi - \Theta$, where $\cos\Theta = \hat{\Omega}' \cdot \hat{\Omega}$, Θ being the scattering angle. When the azimuth angle $\phi = 0°$, the scattering plane coincides with the plane of incidence (the x–z plane).

where the 2π underneath the integral sign indicates integration over the whole hemisphere of incident directions. If the reflected radiance from a diffusely scattering object is the same in all directions of observation $\hat{\Omega}$, regardless of the direction of incidence $\hat{\Omega}'$, it is said to be a Lambert reflector. Then the BRDF simplifies to $\rho(\nu, \hat{\Omega}', \hat{\Omega}) = \rho_L(\nu)$, where $\rho_L(\nu)$ is the Lambert reflectance, and the reflected radiance in Eq. (2) becomes

$$L(\nu, \hat{\Omega}) = \rho_L(\nu) \int_{2\pi} \mathrm{d}\omega' \cos\theta' L(\nu, \hat{\Omega}') = \rho_L(\nu) E(\nu). \quad (3)$$

For a collimated beam (see Fig. 2) with irradiance $E^s(\nu)$ normal to the incident beam direction $\hat{\Omega}_0$, the incident radiance is given by [15]

$$\begin{aligned} L^s(\nu, \hat{\Omega}') &= E^s(\nu)\delta(\hat{\Omega}' - \hat{\Omega}_0) \\ &= E^s(\nu)\delta(\cos\theta' - \cos\theta_0)\delta(\phi' - \phi_0), \end{aligned} \quad (4)$$

and the corresponding incident irradiance is

$$E(\nu, \hat{\Omega}_0) = \int_{2\pi} \mathrm{d}\omega' \cos\theta' L^s(\nu, \hat{\Omega}') = E^s(\nu)\cos\theta_0. \quad (5)$$

From Eqs. (3) and (5), the reflected radiance from a Lambert reflector due to a collimated incident beam is $L(\nu, \hat{\Omega}) = \rho_L(\nu)\cos\theta_0 E^s(\nu)$, and the reflected hemispherical irradiance becomes

$$E(\nu, \hat{\Omega}_0) = \int_{2\pi} \mathrm{d}\omega \cos\theta L(\nu, \hat{\Omega}) = \pi\rho_L(\nu) E^s(\nu)\cos\theta_0. \quad (6)$$

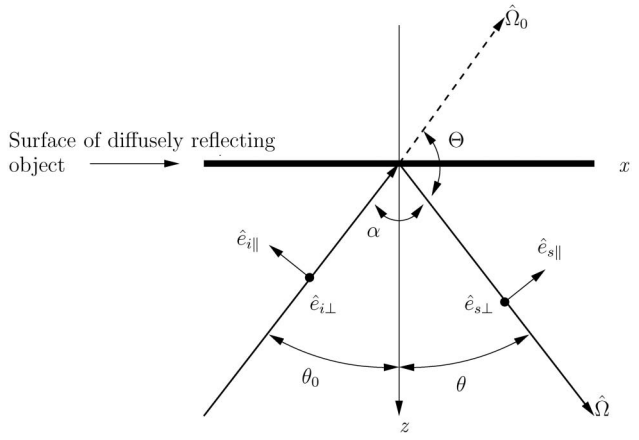

Fig. 2. Schematic of collimated beam scattering geometry. The surface of a diffusely reflecting object lies in the vertical x–y plane, the incident beam is along the unit vector $\hat{\Omega}_0(\theta_0, \phi_0 = 0)$, and the angle of incidence is $\theta_0[0 \le \theta_0 \le 90°]$. The observation direction is along the unit vector $\hat{\Omega}(\theta, \phi)$, and the polar angle of observation is $\theta[-90° \le \theta \le 90°]$. When the azimuth angle of observation $\phi = 0$, the observation direction lies in the plane of incidence (the x–z plane). Note that $\theta = \alpha - \theta_0 = \pi - \Theta - \theta_0$, where Θ is the scattering angle and α is the backscattering angle. The unit vectors $\hat{e}_\parallel$ and the $\hat{e}_\perp$ are parallel and perpendicular, respectively, to the plane of incidence.

Thus, for a Lambert reflector, the ratio of the reflected hemispherical irradiance to the irradiance of the incident collimated beam, called the irradiance reflectance or plane albedo, is given by [15]

$$\rho(\nu, \hat{\Omega}_0, 2\pi) = \frac{E(\nu, \hat{\Omega}_0)}{E^s(\nu)\cos\theta_0} = \pi\rho_L(\nu), \quad (7)$$

where the 2π argument emphasizes the integration over the hemisphere. Because the irradiance reflectance or plane albedo in Eq. (7) must be less than or equal to unity, i.e., $\rho(\nu, \hat{\Omega}_0, 2\pi) \le 1$, a Lambert reflectance must satisfy the inequality $\rho_L(\nu) \le 1/\pi$ for unpolarized light. In practice, it is difficult to realize a reflector with a BRDF that is equal to that of a Lambert reflector for all illumination and observation geometries.

B. Determination of the Incident Irradiance Using Reciprocity

At normal incidence ($\hat{\Omega}_0 = -\hat{z}$), the reflected radiance from a Spectralon reflectance standard is the same for all azimuthal directions so that the reflected hemispherical irradiance becomes

$$E(\nu, -\hat{z}) = 2\pi \int_0^{\pi/2} L^{\mathrm{meas}}(\nu, -\hat{z}, \theta)\cos\theta\sin\theta \mathrm{d}\theta, \quad (8)$$

where $L^{\mathrm{meas}}(\nu, -\hat{z}, \theta)$ is the reflected radiance measured at 5° intervals within the range of observation angles $-90° \le \theta \le 90°$. We determined $E(\nu, -\hat{z})$ by using the measured values of $L^{\mathrm{meas}}(\nu, -\hat{z}, \theta)$ for normal incidence and performing the integration in Eq. (8) numerically by approximating the integral by a sum in accordance with the trapezoidal rule.

The irradiance reflectance or plane albedo is given as the ratio of the reflected hemispherical irradiance $E(\nu, -\hat{z})$ to the incident irradiance $E^s(\nu)$ [see Eq. (7)], i.e.,

$$\rho(\nu, -\hat{z}, 2\pi) = \frac{E(\nu, -\hat{z})}{E^s(\nu)} = 0.98, \quad (9)$$

where the final result in Eq. (9) is in accordance with the manufacturer's specification for the SRS-99-020 Spectralon being examined. Thus, the incident irradiance becomes $E^s(\nu) = E(\nu, -\hat{z})/0.98$.

At normal incidence ($\hat{\Omega}_0 = -\hat{z}$), the BRDF, which, as just mentioned, is independent of the azimuth angle ϕ, is given by

$$\rho(\nu, -\hat{z}, \hat{\Omega}) = \frac{L(\nu, -\hat{z}, \theta, \phi)}{E^s(\nu)} = 0.98\frac{L^{\mathrm{meas}}(\nu, -\hat{z}, \theta)}{E(\nu, -\hat{z})}. \quad (10)$$

The reciprocity principle implies that

$$\rho(\nu, \hat{\Omega}_0, \hat{\Omega}) = \rho(\nu, -\hat{\Omega}, -\hat{\Omega}_0). \quad (11)$$

At non-normal incidence, we have

$$\rho(\nu,\hat{\Omega}_0,+\hat{z}) = \rho(\nu,-\hat{z},-\hat{\Omega}_0) = \rho(\nu,-\hat{z},\theta_0) = 0.98\frac{L^{\text{meas}}(\nu,-\hat{z},\theta_0)}{E(\nu,-\hat{z})}, \quad (12)$$

where the first equality sign follows from reciprocity, the second from the azimuth independence of the BRDF at normal incidence, and the third from Eq. (10), which is based on azimuth independence of the BRDF at normal incidence plus the requirement that the plane albedo be 98%.

From Eq. (1) it follows that the BRDF at non-normal incidence becomes

$$\rho(\nu,\hat{\Omega}_0,\hat{\Omega}) = \frac{\rho(\nu,\hat{\Omega}_0,+\hat{z})}{L^{\text{meas}}(\nu,\hat{\Omega}_0,\hat{z})} + L^{\text{meas}}(\nu,\hat{\Omega}_0,\hat{\Omega}), \quad (13)$$

where the ratio $\rho(\nu,\hat{\Omega}_0,+\hat{z})/L^{\text{meas}}(\nu,\hat{\Omega}_0,\hat{z})$ ensures that the correct value is obtained for $\hat{\Omega}=\hat{z}$. Substituting in Eq. (13) from Eq. (12), we finally have

$$\rho(\nu,\hat{\Omega}_0,\hat{\Omega}) = 0.98\frac{L^{\text{meas}}(\nu,-\hat{z},\theta_0)}{E(\nu,-\hat{z})}\frac{L^{\text{meas}}(\nu,\hat{\Omega}_0,\hat{\Omega})}{L^{\text{meas}}(\nu,\hat{\Omega}_0,\hat{z})}, \quad (14)$$

where $E(\nu,-\hat{z})$ is given in Eq. (8).

C. Polarization Effects

For a polarized collimated beam, we write the BRDF in the following way:

$$\rho_{jk}(\hat{\Omega}_0,\hat{\Omega},\nu) = \frac{L_k(\hat{\Omega}_0,\hat{\Omega})}{E_j^s\cos\theta_0}[\text{sr}^{-1}], \quad (15)$$

where $L_k(\hat{\Omega}_0,\hat{\Omega})$ is the reflected spectral radiance for k polarization in the direction $\hat{\Omega}$ and E_j^s is the incident irradiance normal to the incident beam direction $\hat{\Omega}_0$ for j polarization. The subscripts j and k represent the polarization states of the incident and reflected light, respectively. When $j=u$, the incident light is unpolarized, when $j=s$ or $j=p$, the incident light is polarized perpendicular or parallel to the plane of incidence, which is spanned by $\hat{\Omega}_0$ and $\hat{z}$. For example, when both the incident light and the reflected light are unpolarized, then $j=k=u$, and the BRDF is denoted by ρ_{uu}.

The BRDF due to an electromagnetic beam that illuminates a rough surface [16] depends on the polarization states of both the incident radiation and the observed radiation, each being described by a four element quantity called the Stokes vector $\mathbf{I}=[L_\parallel,L_\perp,U,V]^T$, where the superscript T denotes the transpose. Here $L_\parallel$ and $L_\perp$ are the radiances of the radiation components that are respectively parallel (i.e., along the unit vector $\hat{\mathbf{e}}_\parallel$) and perpendicular (i.e., along the unit vector $\hat{\mathbf{e}}_\perp$) to the plane of incidence, U is the degree of linear polarization in the 45°/135° plane, and V is the degree of circular polarization. The unit vector $\hat{\mathbf{e}}_\perp$ along the normal to the plane of incidence and the unit vector $\hat{\mathbf{e}}_\parallel$, which lies in the plane of incidence but normal to the unit vector $\hat{\mathbf{s}}$ along the propagation direction, are defined such that $\hat{\mathbf{e}}_\perp\times\hat{\mathbf{e}}_\parallel=\hat{\mathbf{s}}$. This Stokes vector representation is related to the more common one $\mathbf{I}_s=[L,Q,U,V]^T$ by $L=L_\parallel+L_\perp$ and $Q=L_\parallel-L_\perp$. When light is scattered by a rough surface, or by a collection of particles, a four-by-four matrix, called the Mueller matrix, provides the linear transformation connecting the Stokes vector of the scattered radiation to that of the incident radiation in the scattering plane, which is spanned by $\hat{\Omega}_0$ and $\hat{\Omega}$. The elements of the Mueller matrix contain information related to the size, shape, and optical properties of the scattering medium. A complete description of the polarized BRDF requires all elements of the Mueller matrix. However, the orthogonal states of plane-polarized light, which form a 2×2 submatrix in the upper-left corner of the Mueller matrix, determines the polarizance [the degree to which incident unpolarized light becomes polarized into the parallel (p) and perpendicular (s) states].

We have taken a simplified approach to electromagnetic scattering by a diffusely reflecting object in which we considered the radiation incident upon the object to contain (i) only parallel polarization represented by the component $L_\parallel^i$, (ii) only perpendicular polarization represented by the component $L_\perp^i$, and (iii) unpolarized light represented by half the sum of $L_\parallel^i$ and $L_\perp^i$. In each of these cases, we detected both $L_\parallel^{\text{sc}}$ and $L_\perp^{\text{sc}}$, where $L_\parallel^{\text{sc}}$ and $L_\perp^{\text{sc}}$ stand for the parallel ($p=\parallel$) and the perpendicular ($s=\perp$) radiance components of the scattered light. To characterize the polarization state of the scattered light, we employed the degree of reduced linear polarization P of the scattered light, which is obtained by neglecting the U component of the Stokes vector, i.e.,

$$P = \frac{|Q^{\text{sc}}|}{L^{\text{sc}}} = \frac{|L_\parallel^{\text{sc}}-L_\perp^{\text{sc}}|}{L_\parallel^{\text{sc}}+L_\perp^{\text{sc}}}, \quad (16)$$

where the superscript sc stands for scattered light. If $P=1$, the scattered light is completely polarized, and if $P=0$, the scattered light is unpolarized. Therefore, P is bounded within the interval $0\le P\le1$ for partially polarized light. The measurement of the degree of polarization defined as $P=\sqrt{(Q^{\text{sc}})^2+(U^{\text{sc}})^2+(V^{\text{sc}})^2}/L$, is beyond the scope of this paper.

The change of polarization due to rough-surface scattering was studied by Torrance *et al.* [17] using a microfacet surface model. They showed experimentally that the angular distribution of plane-polarized incident light reflected from a rough surface varied with the angle of incidence, and that a Lambertian type of reflector was obtained only for normal incidence, as predicted by the microfacet model. Deboo *et al.* [18] measured the degree of polarization P

for scattering of polarized light by artificial rough surfaces and showed that it varied with the observation direction and had a maximum value near the normal direction of observation. Haner *et al.* [9] measured the BRDF of Spectralon white reflectance standards using coherent, polarized laser light, and showed that the BRDF as well as P increased as the observation angle increased toward that of the specular direction in the plane of incidence. Enhancement of backscattering from rough surfaces has been studied both numerically [19] and experimentally [20–22]. Recently, Simonsen *et al.* [23] simulated the scattering of p-polarized light from metallic and dielectric rough surfaces and showed that the backscattered light intensity in the plane of incidence was enhanced compared to that in a plane normal to the plane of incidence. These simulations included only rough-surface scattering, whereas the Spectralon standard is expected to behave mainly as a volume scatterer [9] due to multiple-scattering events taking place beneath its surface.

2. Experimental Setup

A. Light Source and Detector

A quasi-monochromatic incoherent beam of light, at a wavelength of 405 nm or 680 nm, was generated from a LQX 1000 xenon lamp (LINOS Photonics GmbH, Munich, Germany) by using an interference bandpass filter (IF in Fig. 3) (Andover Corporation, Salem, N.H.) with a bandwidth of 10 nm. As illustrated in Fig. 3, the beam of light was collimated by lens L and reflected from mirror M in order to illuminate the Spectralon surface at a given angle of incidence. The beam of light from the xenon lamp was unpolarized, but to account for possible polarization effects due to its transmission through various optical components, we measured the p and s polarization components of the collimated beam by polarizer P (see Fig. 3) and evaluated the degree of reduced linear polarization P using the definition in Eq. (16). It was found that the polarization of the collimated beam was about 10% and 15% at 680 and 405 nm, respectively. We used a xenon lamp in order to avoid speckles in the BRDF profiles. Figure 4 shows the Spectralon BRDF measured at normal incidence ($\theta_0 = 0$; see Fig. 2) using both a 670 nm diode laser (LDM145G, Imatronics, Gwent UK) and a xenon lamp with a bandpass filter centered at 670 nm. The speckle effects due to coherent laser light are seen to give a BRDF that can deviate by as much as 2.5% from that measured using an incoherent xenon lamp for observation angles θ within the range $-60° \le \theta \le 60°$ (see Fig. 2). The speckle effects can vary depending on the observation angle and the angle of incidence [10].

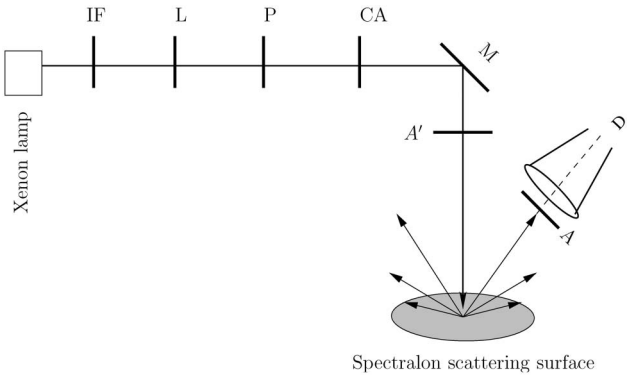

Fig. 3. Sketch of optical setup in the experiment: IF, interference filter; L, lens; P, polarizer; CA, circular aperture; M, plane mirror; A′, temporary analyzer; A, analyzer; D, detector. Note that the Spectralon scattering surface is aligned parallel to the vertical plane.

The detector was a silicon-based photodiode power optometer (S370 Graseby Optics). It had an active sensing area of 1 cm^2 giving 0.14 to 0.40 A per watt absolute responsivity in the visible range. The detector was mounted on a computer-controlled goniometer arm at a distance of 300 mm from the center of the goniometer circle. The scattered light from the illuminated surface area was focused onto the detector using a lens (not shown in Fig. 3) with a 26 mm effective diameter and 30 mm focal length through a 2 mm circular aperture immediately in front of the detector. We assumed the beam divergence to be negligible. The detector aperture subtended a solid angle at the lens larger than that subtended by the illuminated surface area (of diameter ≤10 mm) so that the light reflected back from the illuminated Spectralon sample to the lens was collected by the sensing area of the detector.

B. Measurements and Analyses

A schematic of the optical setup of the goniometer system is shown in Fig. 3, and a detailed description of this goniometer setup is given in Zhao *et al.* [24]. During the measurements we placed the Spectralon reflecting surface in the vertical plane (the x–y plane

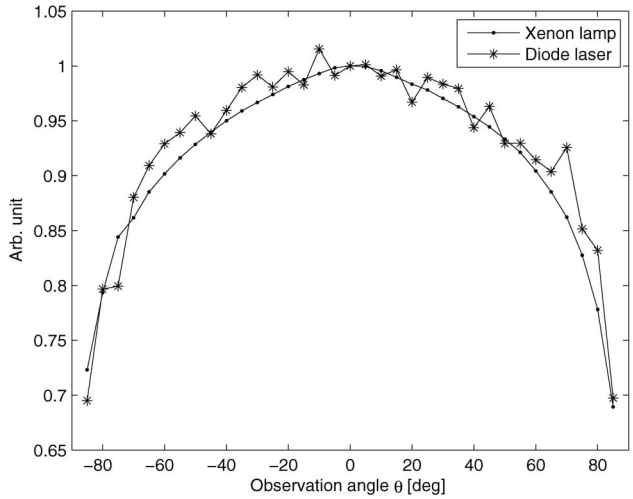

Fig. 4. Spectralon BRDF curves (ρ_{uu}) measured at 670 nm for unpolarized illumination from a xenon lamp (•–) and for illumination from a 670 nm diode laser (∗–) at $\theta_0 = 0°$ [see Figure 2]. The curves are normalized to 1 at $\theta = 0°$.

in Fig. 2) at the center of the goniometer ring to make it possible for the detector to measure reflected light for observation angles in the range $-90° \le \theta \le 90°$ (see Fig. 2). Some of the measurements were made in the plane of incidence ($\phi = \phi_0 = 0°$), but most of them were made by lifting the detector tube 6° above the plane of incidence (the x–z plane in Fig. 2) so that the lifted detector could detect the scattered light within the entire range of observation polar angles by avoiding the obscurity due to the position of mirror. However, in this lifted observation plane, it was not possible to detect the scattered light in the direction of specular reflection ($\theta = \theta_0$, $\phi = \phi_0 = 0°$). On the other hand, with measurements in the plane of incidence, it was not possible to detect the backscattered light in directions close to that opposite to the direction of incidence ($\theta = -\theta_0$, $\phi = \phi_0 = 0°$) due to the shadow of the mirror.

To obtain the reflected radiance L for an incident irradiance E, the power [W] of the reflected light was measured for different angular positions of the detector and divided by the solid angle subtended by the detector to obtain L[W m^{-2} sr^{-1}]. The solid angle subtended by the detector was given by $(r/R)^2\pi\cos\theta$, where r is the radius of the aperture of the lens mounted in front of the detector, R is the distance from the illuminated area on the Spectralon surface at the center of the goniometer to the lens, and θ represents the angular position of the detector.

Our analyses relied on the assumptions that the Spectralon reflection standard had 98% irradiance reflectance, as given by the manufacturer, and that the reflected radiance was azimuth independent for normal incidence. In contrast to the latter assumption, the measurements for normally incident polarized light with the detector lifted 6° above the plane of incidence were not perfectly symmetrical about $\theta = 0$. At 405 nm, the maximum asymmetry for *ss* polarization was found to occur for the measured value at $\theta = -50°$, which was 6% higher than at $\theta = +50°$. At 680 nm, the maximum asymmetry was 7% for *ss* polarization, but less than 5% for *pp* polarization. In order to compensate for this asymmetry, which was assumed to be due to measurement errors, the measured radiance values for normal incidence were symmetrized by setting $L_{\mathrm{sym}}(\theta) = L_{\mathrm{sym}}(-\theta) = \frac{1}{2}[L_{\mathrm{sym}}(-\theta) + L_{\mathrm{sym}}(\theta)]$. This symmetrized $L_{\mathrm{sym}}(\theta)$ function was assumed to be azimuth independent, and it was therefore used to calculate E as explained in Subsection 1.B. For normal incidence, the BRDF, which is equal to L_{sym}/E[sr^{-1}], was calculated as described in Eq. (1). All measurements of the BRDF for non-normal incidence were normalized by use of the reciprocity theorem, as explained in Subsection 1.B.

For measurements made when the detector tube was lifted 6° above the x–z plane in Fig. 2, the angles (θ_g, ϕ_g) in the goniometer coordinate system and the angles (θ, ϕ) in the Spectralon reflection standard coordinate system are related by

$$\theta = \begin{cases} \arccos(\cos\theta_g \cos\phi_g) & \text{for } \theta_g \ge 0 \\ -\arccos(\cos\theta_g \cos\phi_g) & \text{for } \theta_g < 0 \end{cases}, \tag{17}$$

$$\phi = \begin{cases} \arcsin\left[\frac{\sin\phi_g}{[1-(\cos\theta_g\cos\phi_g)^2]^{1/2}}\right] & \text{for } \theta_g \ge 0 \\ \pi + \arcsin\left[-\frac{\sin\phi_g}{[1-(\cos\theta_g\cos\phi_g)^2]^{1/2}}\right] & \text{for } \theta_g < 0 \end{cases}. \tag{18}$$

Thus, the measured power of the reflected light was corrected through division by $\cos\theta$, with θ as given in Eq. (17), but for $\cos\phi_g = \cos 6° = 0.995$, the difference between $\cos\theta = \cos\theta_g\cos\phi_g$ and $\cos\theta_g$ is negligible.

1. *Alignment and Repeatability*

To align the optical setup, we let a collimated unpolarized beam at a wavelength of 680 nm be normally incident on the central area of the Spectralon surface, so that $\theta_0 = 0$ in Fig. 2. Next, we carefully aligned the Spectralon surface so as to obtain a symmetrical angular distribution of the reflected light about the surface normal, i.e., to obtain the same reflected radiance for $\theta = -\theta_0$ and $\theta = +\theta_0$, which is true for normally incident light.

Measurements were made at observation angles θ at every 5° interval. In each measurement, the detector recorded 10 raw data sets, each for an integration time of 100 ms, and the median value, which had a relative standard deviation ≤1.3%, was used to obtain the BRDF. The background noise due to the ambient light and the detector dark current was measured to be in the order of 10^{-12} W. In order to check the measurement repeatability, we repeated five measurements at normal incidence ($\theta_0 = 0°$ in Fig. 2) without altering the setup and compared these measurements as shown in Fig. 5. The goniometer system showed repeatable results with root mean square (rms) values that were less than 1% for observation angles θ in the range $-80° \le \theta \le +80°$.

2. *Homogeneity of Spectralon Surface*

The selected Spectralon white reflectance standard SRS-99-020 (Labsphere, Inc., North Sutton, N.H.) had a flat circular reflecting surface with a diameter of 50.8 mm (the total dimensions were 60.45 mm in diameter and 15.24 mm in height). We checked the homogeneity of the surface by measuring reflected light from five different equally large neighboring patches (each about 8 mm in diameter) that were illuminated at normal incidence ($\theta_0 = 0°$ in Fig. 2). First we measured reflected light from the central area for observation angles θ in the range $-85° \le \theta \le +85°$, and then we translated the Spectralon surface about 10 mm vertically (up and down) and horizontally (left and right) to measure reflected light from four additional surface patches. These measurements, which are compared in Fig. 6, showed that the variations in reflected light from the five different surface patches were fairly close

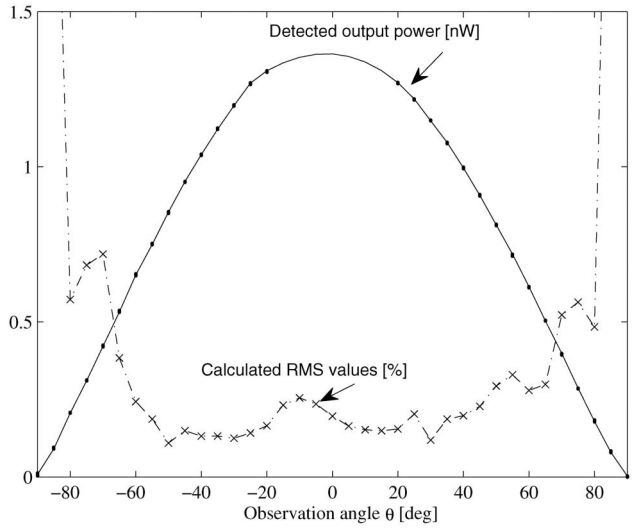

Fig. 5. Raw data averages and rms values obtained from test measurements at normal incidence ($\theta_0 = 0°$ in Fig. 2) to examine the repeatability of measured results. Bullets (•) and crosses (×) indicate measured values between which there is linear interpolation, except between the values for $\theta = -20°$ and $\theta = +20°$, in which case spline interpolation was used. The units on the left vertical axis represent the percentage rms values and the detected average output power in nanowatts.

to the rms value, i.e., less than 1% for observation angles θ in the range $-65° \le \theta \le +65°$. However, at larger observation angles, the rms value increased, which may be due to a decreasing signal-to-noise ratio.

3. *Polarization States*

We measured the BRDF in the plane of incidence and 6° above it for various combinations of polarization states for the incident and detected light for six different angles of incidence: $\theta_0 = 0°$, 20°, 30°, 38°, 45°, and 60°. The orthogonal polarization states $L_\parallel$ and $L_\perp$ are denoted by p and s, respectively, and unpolarized light is denoted by u. Seven different combinations of polarization states for the incident and detected light were investigated. These are denoted by uu, ss, sp, pp, ps, su, pu, where the first and last letter of each combination indicate the polarization state of the incident and detected light, respectively. The s- and p-polarization components of the incident light were carefully checked in each measurement with an analyzer temporarily placed between the reflecting mirror and the Spectralon surface (see Fig. 3). As explained in Section 1, the Spectralon surface is nonabsorbing and does not produce fluorescence effects in the visible and near-infrared spectral ranges, so that the scattering is conservative, and the reflected radiance is nearly Lambertian at normal incidence for which $\theta_0 = 0°$ Fig. 2.

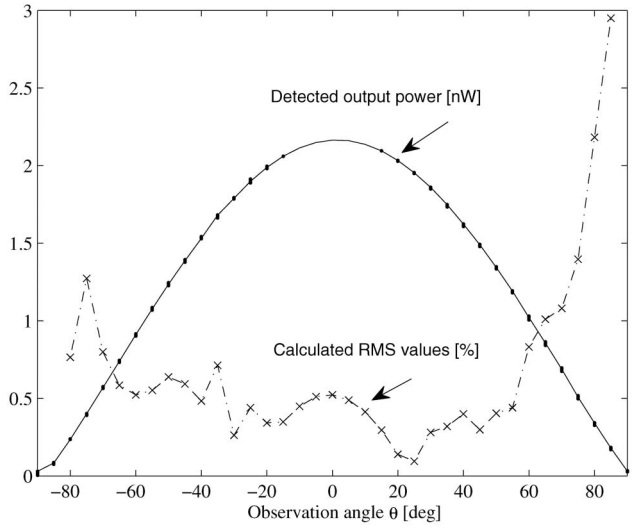

Fig. 6. Raw data averages and rms values for measurements at normal incidence ($\theta_0 = 0°$) on the Spectralon test material at five different areas. Bullets (•) and crosses (×) indicate measured values between which there is linear interpolation, except between the values for $\theta = -20°$ and $\theta = +20°$, in which case spline interpolation was used. The units on the left vertical axis represent the percentage rms values and the detected output power in nanowatts.

3. Results and Discussion

In this section, we compare measured Spectralon BRDF curves with the Lambertian BRDF for various angles of incidence and various combinations of polarization states of the incident and detected light. For each angle of incidence θ_0, we plot the measured BRDF and the corresponding degree of linear polarization P [see Eq. (16)] against the observation angle θ in the range $-90° \le \theta \le +90°$.

The BRDF curves in Figs. 7 and 8 are for a wavelength of 680 nm, measured in the plane of incidence (Fig. 7) and in an observation plane that was 6° above the plane of incidence (Fig. 8), while those in Fig. 9 are for a wavelength of 405 nm measured in an observation plane that was 6° above the plane of incidence. In Fig. 7 there are four panels (a)–(d) corresponding to angles of incidence of $\theta_0 = 0°$,30°, 45°, and 60°, respectively, whereas Figs. 8 and 9 contain six panels (a)–(f) corresponding to angles of incidence of $\theta_0 = 0°$, 20°, 30°, 38°, 45°, and 60°, respectively. Each panel in Figs. 7–9 contains seven BRDF curves, each curve representing a particular combination of polarization states for the incident and detected light, i.e., uu, ss, sp, pp, ps, su, and pu, where the first and last letter of each combination indicate the polarization states of the incident and detected light, respectively. The color codes used in Figs. 7–9 are as follows: (black −curve) $\rightarrow uu/2$, (blue −curve) $\rightarrow ss$, (blue − • curve) $\rightarrow sp$, (red −curve) $\rightarrow pp$, (red − • curve) $\rightarrow ps$, (green −curve) $\rightarrow su/2$, and (green − • curve) $\rightarrow pu/2$. Note that each of the uu BRDF curves, which is equal to $1/\pi$ for a Lambert reflector, has been divided by 2 for comparison with the polarized BRDF curves, each of which having the value $1/2\pi$ (represented by the symbols × in Figs. 7–9) for a Lambert reflector.

The BRDF curves measured in the plane of incidence (Fig. 7) did not reveal any specular reflection component at any of the four different angles of

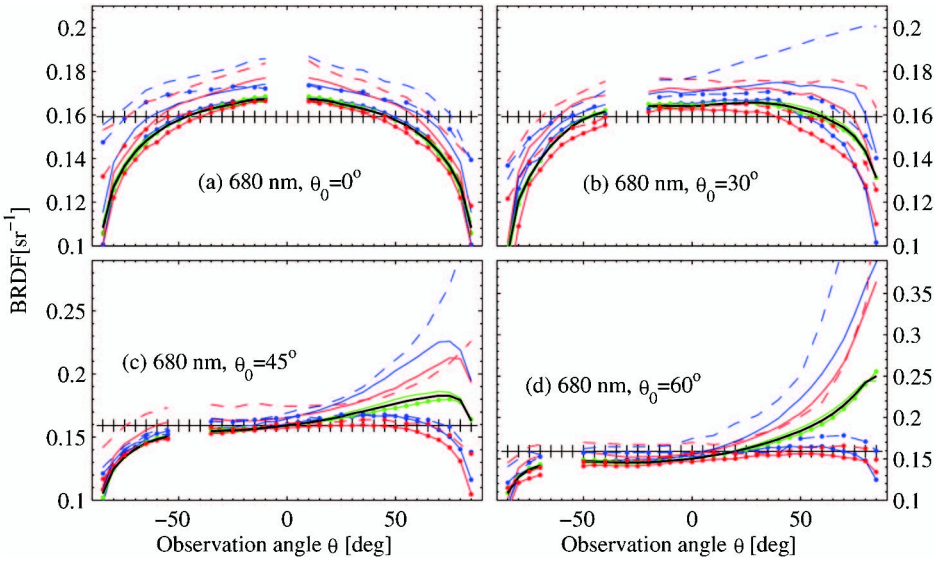

Fig. 7. Spectralon BRDF curves measured in the plane of incidence at a wavelength of 680 nm for angles of incidence θ_0 as indicated in each of parts (a)–(d). Curves with blue or red color represent s or p polarization, respectively, of the incident light. For each polarization state of the incident light, both the copolarized component (indicated by –) and the cross-polarized component (indicated by –•) are presented. The green curves represent unpolarized detected light, i.e., measurements in which there was no analyzer in front of the detector, and in this case the symbols – and –• are used to indicate s and p polarization, respectively, of the incident light. The black symbols × along the horizontal axis show the Lambertian BRDF, and the black – curves show the BRDF for the case uu of unpolarized incident and detected light. Thus, [– → $uu/2$ (black)], [– → ss (blue)], [–• → sp (blue)], [– → pp (red)], [–• → ps (red)], [– → $su/2$ (green)], and [–• → $pu/2$ (green)]. For comparison, BRDF curves at 632.8 nm, measured by Haner *et al.* [9] are represented by [–– → ss (blue)], [– • – → sp (blue)], [–– → pp (red)], [– • – → ps (red)]. Note that the test sample of Haner *et al.* [9] was different from ours.

incidence, but revealed a gradual increase of scattering for $\theta > 0$ as the angle of incidence θ_0 got larger.

We expected the Spectralon reflectance standard to have a nearly Lambertian BRDF at normal incidence ($\theta_0 = 0°$). But Fig. 7 (pertaining to the plane of incidence) as well as Figs. 8(a) and 9(a) (pertaining to an observation plane that was 6° above the plane of incidence) show deviations from Lambertian behavior even for small absolute values of the observation angle θ. The deviation from Lambertian behavior varies with $|\theta|$, both for $\theta < 0$ and $\theta > 0$. In the case of normal incidence and unpolarized incident and detected light [see black – curve in Fig. 7(a)], the measured BRDF is found to be $\simeq$5% higher than the Lambertian BRDF when $|\theta| \le 50°$, but to be 20% below the Lambertian BRDF when $|\theta| > 60°$. Similarly, at normal incidence, the relative difference between the uu BRDF values measured in the plane of incidence and in an observation plane that was 6° above the plane of incidence was found to be about 3% for observation angles in the range $-60° \le \theta \le 60°$, but to be more than 3% for $\theta > 60°$.

The dashed curves in Fig. 7 are BRDF curves for polarized light measured by Haner *et al.* [9] from position 1 of Spectralon test sample number 12,969. These curves show that the measured BRDF for polarized incident light is generally higher than the Lambertian BRDF value of $1/2\pi$ for polarized light. For small absolute values of the observation angle θ, the copolarized BRDF curves of Haner *et al.* [9] are seen to be 15% higher than the Lambertian BRDF, whereas the corresponding difference found from our measurements is about 10%. Moreover, such differences are seen to increase more for $\theta > 0$ as the angle of incidence θ_0 increases. The difference of about 5% between our measurements and those of Haner *et al.* [9] may be due to difference in surface finish between the Spectralon samples.

At an angle of incidence of $\theta_0 = 20°$, all BRDF components in Figs. 8(b) and 9(b) are slightly enhanced for $\theta > 0$, and when $\theta_0 = 30°$, all copolarized components of the BRDF are further enhanced for $\theta > 0$, while the uu component is found to lie between the copolarized and the cross-polarized components. Enhanced scattering for $\theta > 0$ is seen to occur for $\theta_0 > 38°$. At an angle of incidence of $\theta_0 = 38°$, the copolarized BRDF components in Figs. 8 and 9 as well as the uu component exceed the Lambertian BRDF in observation directions with $\theta > 0$. Furthermore, the ss component of the BRDF is seen to be the largest of all BRDF components in observation directions with $\theta < 0$. For $\theta_0 \ge 45°$, enhanced scattering for $\theta < 0$ of the pp component is seen both at 680 nm (Fig. 8) and at 405 nm (Fig. 9), but more pronounced in the former case. At $\theta_0 = 60°$, the copolarized and unpolarized BRDF components exceed the Lambertian BRDF for $\theta > 0$. Also for $\theta_0 \ge 20°$, the ss components of the BRDF [blue – curves in panels (b)–(f) in Figs. 7–9] are seen to have stronger enhanced scattering for $\theta > 0$ than the pp components (red – curves in the same figures). For larger θ_0, the difference between the two cross-polarized components (blue – • →sp and red – • →ps) increases as the

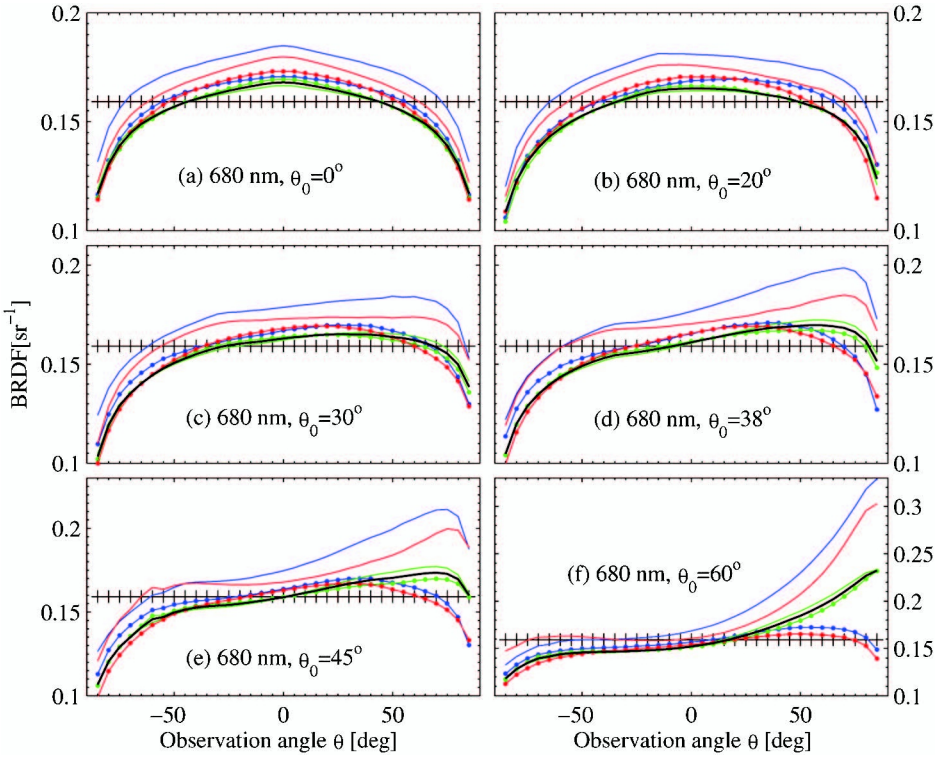

Fig. 8. Spectralon BRDF curves measured in an observation plane that was 6° above the plane of incidence at a wavelength of 680 nm for angles of incidence θ_0 as indicated in each of parts (a)–(f). Curves with blue or red color represent s or p polarization, respectively, of the incident light. For each of these polarization states of the incident light, both the copolarized component (indicated by –) and the cross-polarized component (indicated by –•) are presented. The green curves represent unpolarized detected light, i.e., measurements in which there was no polarizer in front of the detector, and in this case the symbols – and –• are used to indicate s and p polarization, respectively, of the incident light. The black symbols × along the horizontal axis show the Lambertian BRDF, and the black – curves show the BRDF for the uu case of unpolarized incident and detected light. Thus, [– → $uu/2$ (black)], [– → ss (blue)], [–• → sp (blue)], [– → pp (red)], [–• → ps (red)], [– → $su/2$ (green)], and [–• → $pu/2$ (green)].

observation angle θ increases for $\theta > 0$. Such differences are seen to be larger at 405 nm than at 680 nm.

The ratio of BRDF components for polarized light at 680 nm measured in the plane of incidence (Fig. 7) to those measured in an observation plane that was 6° above the plane of incidence (Fig. 8) was examined for four different angles of incidence θ_0 (not shown here). This ratio should be equal to 1, if the Spectralon surface were a perfect Lambert surface, but was found to deviate from 1 as $|\theta|$ increased, and the deviation was found to be larger for the copolarized components than for the cross-polarized components. Within the range of observation angles $-60° \le \theta \le 60°$, the difference between the BRDF components for polarized light at 680 nm measured in the plane of incidence and in an observation plane that was 6° above the plane of incidence was found to be ≤5%, which is close to the corresponding difference found in the uu case of unpolarized illumination and detection.

Figures 7–9, which show the variation of the BRDF components with the observation angle θ, indicate that the anisotropic characteristics of the scattering increase with the angle of incidence θ_0. For largeangles of incidence, all BRDF curves show enhanced scattering in observation directions with $\theta > 0$. Also, slightly enhanced scattering is observed for $\theta < 0$ for p-polarized incident light for $\theta_0 \ge 38°$. Such scattering events may be related to the geometric self-shadowing and self-masking [25] caused by the surface topography as well as multiple-scattering effects [13,23] that occur on the surface as well as in the region below it.

If the structure of the Spectralon standard were such as to scatter the incident light uniformly in all directions, the hemispherical distribution of the scattered light would follow the Lambert cosine law. In practice, Lambertian reflectors do not exist, but the Spectralon standard, which has the most superior diffuse reflectance of any known light-diffusing material, is assumed to behave nearly Lambertian [1] in the UV, visible, and near-infrared spectral ranges, covering wavelengths from 0.257 to 10.6 μm. If it were so, the measured BRDF curves would be almost independent of the viewing direction. However, The BRDF curves in Figs. 7–9 for the Spectralon standard show deviations from the ideal Lambertian BRDF values as a function of the observation angle θ for various angles of incidence θ_0, and these deviations also depend on the polarization states of the incident and detected light.

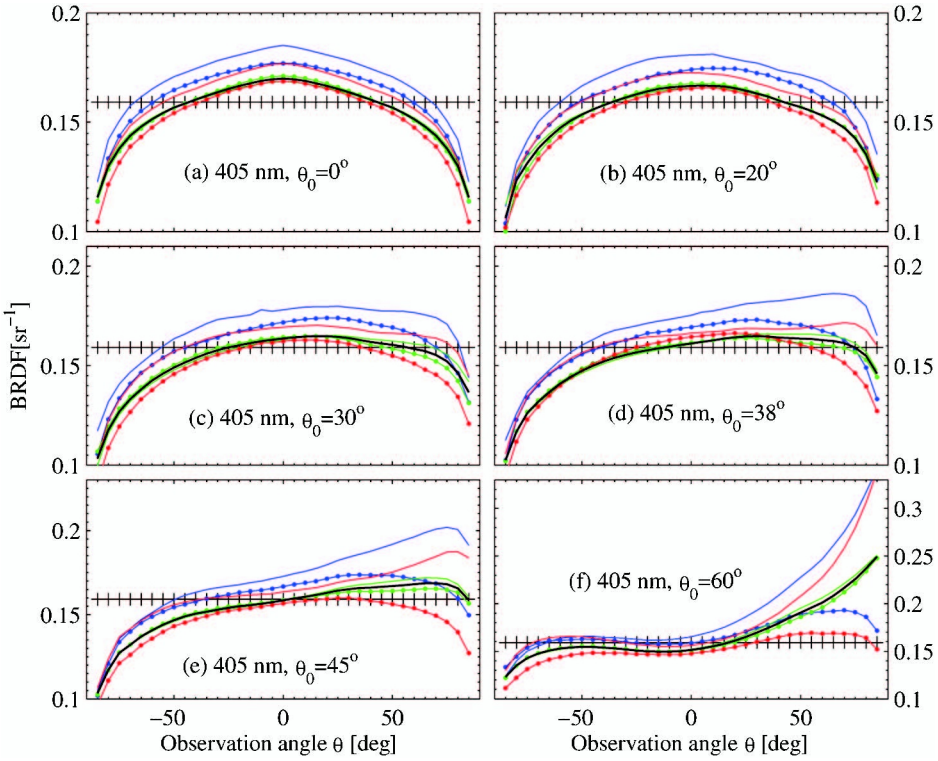

Fig. 9. Symbols and legends are the same as in Fig. 8 except that the wavelength of the incident light was 405 nm for the results shown in this figure.

In our measurements as well as in those of Haner *et al.* [9], the *s*-polarized BRDF is always greater than the *p*-polarized BRDF for $\theta > 0$, whereas for large angles of incidence [see Figs. 8(e), 8(f), 9(e), and 9(f)], the opposite is seen to be true for $\theta < 0$. Comparison of BRDF curves for polarized light measured in the plane of incidence (Fig. 7) and 6° above it (Fig. 8) indicates that enhanced scattering for $\theta < 0$ occurs more in the plane of incidence than in other observation planes. However, as pointed out previously, scattering for $\theta < 0$ in directions close to the direction opposite to that of incidence was not possible to detect due to obscuration by the detector.

Figure 10 shows the degree of reduced linear polarization P versus observation angle θ for six different angles of incidence, computed from Eq. (16) based on the results shown in Figs. 8 and 9. Our measured results in Fig. 10 show that polarized incident light gets more depolarized due to scattering by the Spectralon at small angles of incidence θ_0 than at large values of θ_0. At normal incidence, Fig. 10(a) shows that 680 nm *s*-polarized incident light gives higher P values ($\simeq$5%) than for *p*-polarized incident light. For $\theta_0 \geq 30°$, the P values for *s*-polarized incident light are found to increase with θ for $\theta > 0$, while the P value for *p*-polarized incident light decreases to a minimum close to the direction of normal observation ($\theta = 0°$), and then it increases with θ for $\theta > 0$ more than it does for $\theta < 0$. This behavior suggests that the randomization due to scattering of the incident light from Spectralon is polarization dependent, so that *p*-polarized incident light becomes more depolarized by scattering from the Spectralon standard than *s*-polarized light.

By comparing the P values at 405 and 680 nm in Fig. 10, we see that for *s*-polarized incident light they are larger at 680 nm than at 405 nm when $\theta_0 \leq 45°$, while they are found to be close to each other in the range of observation angles $-50° \leq \theta \leq 25°$ when $\theta_0 = 60°$. For *p*-polarized incident light, the P values are smaller at 680 than at 405 nm for small angles of incidence ($\theta_0 = 0°$–$20°$), are about the same at the two wavelengths for intermediate angles of incidence ($\theta_0 = 30°$–$38°$), and are larger at 680 nm than at 405 nm for large angles of incidence ($\theta_0 = 60°$) [see Fig. 10(f)]. Thus, the depolarization of polarized incident light due to scattering from the Spectralon standard depends on the wavelength of the incident light and the angle of incidence.

The influence of the wavelength of the incident light on the BRDF due to rough-surface scattering can be related to a Rayleigh criterion [26], according to which a rough surface will reflect specularly if the wavelength of the incident light is large compared to the surface roughness. Similarly, the strong scattering in directions with $\theta > 0$ [see Figs. 8(f) and 9(f)] can be intuitively explained in terms of another Rayleigh criterion [27,28], according to which a surface will behave smoother for small grazing angles $\beta = \pi/2 - \theta_0$ (θ_0 is the angle of incidence) than for large grazing angles. These criteria are based on surface topography and do not take into account that the incident light undergoes multiple reflections underneath the Spectralon surface. Also, neither of these

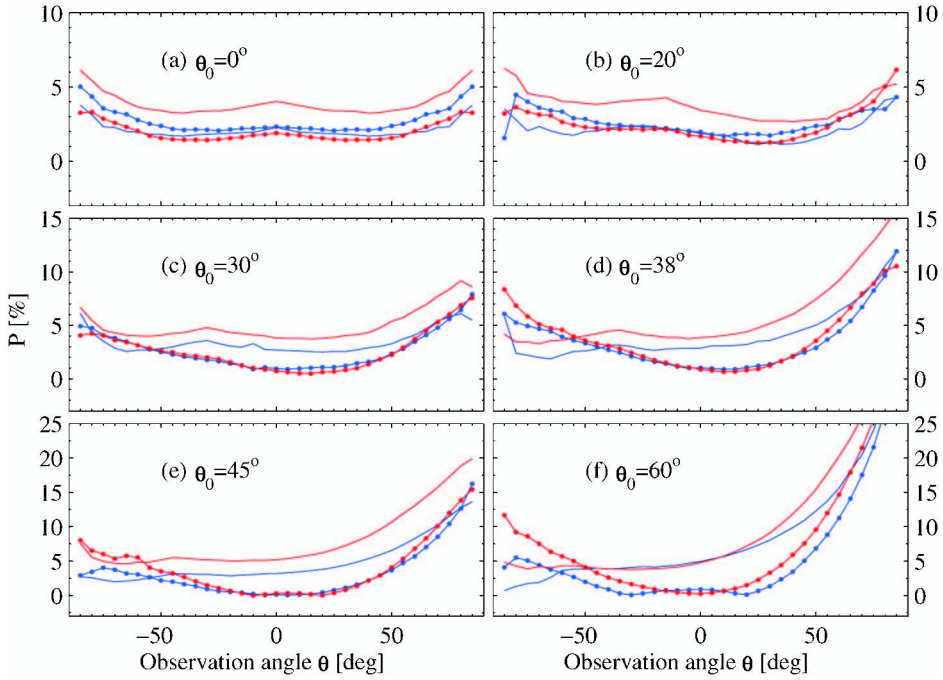

Fig. 10. Degree of reduced linear polarization P (in percent) versus observation angle θ for different angles of incidence θ_0 as indicated in panels (a)–(f). The blue and red curves represent incident light at 405 and 680 nm, respectively, and the degree of reduced linear polarization P is represented by the symbol – for s-polarized incident light and by –• for p-polarized incident light. Thus, – → s-polarized incident light at 405 nm, –• → p-polarized incident light at 405 nm, – → s-polarized incident light of 680 nm, and –• → p-polarized incident light at 680 nm.

two Rayleigh criteria refers to the polarization state of the incident light.

Our results show that the difference between scattering at 405 and at 680 nm is larger for s-polarized incident light than for p-polarized incident light. At normal incidence, both s- and p-polarized light have electric field vectors that are parallel to the flat surface plane. However, at oblique incidence, self-shadowing masking effects [17,25] due to surface microtopography may reduce the amount of scattered light and the direction of the electric field vector for p-polarized light relative to the flat surface plane, and more importantly, relative to the plane of a rough-surface facet, depends on the angle of incidence, resulting in a partial conversion from p- to s-polarized incident light with respect to reflection from the facets. In contrast, the orientation of the electric field vector for s-polarized incident light will remain the same relative to the flat surface plane or the rough-surface facet planes at all angles of incidence. This conversion may contribute to explain our observation noted above that as the angle of incidence gets sufficiently large ($\theta_0 \geq 45°$), the magnitudes of the different BRDF components are found to be such that $ss > pp > su > uu > pu > sp > ps$ for $\theta > 0$.

Light scattering from a Spectralon standard is probably dominated by volume scattering occurring beneath its surface, whose complete description requires the use of Mueller matrices [13,29], which is beyond the scope of this paper. In the case of single scattering within the volume, the reflected light may retain its original state of polarization, but in the case of multiple scattering within the volume, the reflected light is likely to have a different state of polarization than the incident light. Therefore, measurements of copolarized light, which include both singly scattered and multiply scattered light, have higher BRDF values than measurements of cross-polarized light.

4. Conclusions

We have measured the BRDF for a Spectralon white reflectance standard in the plane of incidence and in an observation plane 6° above the plane of the incidence by illuminating it at different angles of incidence with unpolarized and plane-polarized light at 680 and 405 nm. At normal incidence, the difference between the BRDF measured in the plane of incidence and in an observation plane 6° above it was found to be about ≤5% for observation angles θ in the range $-60° \leq \theta \leq 60°$. At large angles of incidence, this difference was found to be larger.

The BRDF of the Spectralon white reflectance standard was found to deviate considerably from the Lambertian BRDF. Thus, all polarization components of the measured BRDF were found to vary with the angle of observation, and the anisotropic angular scattering characteristics were found to vary with both the angle of incidence and the states of polarization of the incident and detected light. Therefore, for the purpose of calibration, the Spectralon BRDF should be measured at all relevant angles of

incidence and for all relevant combinations of the polarization states of the incident and detected light.

This work was financially supported by the Norwegian Research Council. We are grateful to Balter Medical AS, Bergen, Norway for technical support and to two anonymous reviewers for comments and suggestions on how to improve the paper.

References

1. "A guide to reflectance coatings & materials," http://www.pro-lite.co.uk/File/Tech_guide_coatings_&_materials.pdf.
2. B. Gordon, "Integrating sphere diffuse reflectance technology for use with UV-visible spectroscopy," Tech. Note 51450 (Thermo Fisher Scientific, 2007).
3. "Reflectance standards product sheet_8.pdf," http://www.labsphere.com/data/userFiles/.
4. K. Stamnes, B. Hamre, J. J. Stamnes, G. Ryzhikov, M. Biryulina, R. Mahoney, B. Haus, and A. Sei, "Modeling of radiation transport in coupled atmosphere-snow-ice-ocean systems," J. Quant. Spectrosc. Radiat. Transfer **112**, 714–726 (2011).
5. D. A. Haner, B. T. McGuckin, R. T. Menzies, C. J. Bruegge, and V. Duval, "Directional-hemispherical reflectance for Spectralon by integration of its bidirectional reflectance," Appl. Opt. **37**, 3996–3999 (1998).
6. K. J. Voss and H. Zhang, "Bidirectional reflectance of dry and submerged Labsphere Spectralon plaque," Appl. Opt. **45**, 7924–7927 (2006).
7. E. A. Early, P. Y. Barnes, B. C. Johnson, J. J. Butler, C. J. Bruegge, S. F. Biggar, P. R. Spyak, and M. M. Pavlov, "Bidirectional reflectance round-robin in support of the Earth Observing System program," Am. Met. Soc. **17**, 1078–1091 (2000).
8. G. T. Georgiev and J. J. Butler, "Long-term calibration monitoring of Spectralon diffusers BRDF in the air-ultraviolet," Appl. Opt. **46**, 7892–7898 (2007).
9. D. A. Haner, B. T. McGuckin, and C. J. Bruegge, "Polarization characteristics of Spectralon illuminated by coherent light," Appl. Opt. **38**, 6350–6356 (1999).
10. G. T. Georgiev and J. J. Butler, "The effect of speckle on BRDF measurements," Proc. SPIE **5882**, 588203 (2005).
11. B. T. McGuckin, D. A. Haner, R. T. Menzies, C. Esproles, and A. M. Brothers, "Directional reflectance characterization facility and measurement methodology," Appl. Opt. **35**, 4827–4834 (1996).
12. G. T. Georgiev and J. J. Butler, "The effect of incident light polarization on Spectralon BRDF measurements," Proc. SPIE **5570**, 492–500 (2004).
13. T. A. Germer, "Polarized light diffusely scattered under smooth and rough interfaces," Proc. SPIE **5158**, 193204 (2003).
14. F. E. Nicodemus, "Reflectance nomenclature and directional reflectance and emissivity," Appl. Opt. **9**, 1474–1475 (1970).
15. G. Thomas and K. Stamnes, *Radiative Transfer in the Atmosphere and Ocean* (Cambridge University, 1999).
16. D. S. Flynn and C. Alexander, "Polarized surface scattering expressed in terms of a bidirectional reflectance distribution function matrix," Opt. Eng. **34**, 1646–1650 (1995).
17. K. E. Torrance, E. M. Sparrow, and R. C. Birkebak, "Polarization, directional distribution and off-specular peak phenomena in light reflected from roughed surfaces," J. Opt. Soc. Am. **56**, 916–925 (1966).
18. B. J. DeBoo, J. M. Sasian, and R. A. Chipman, "Depolarization of diffusely reflecting man-made objects," Appl. Opt. **44**, 5434–5444 (2005).
19. D. Torrungrueng and J. T. Johnson, "Numerical studies of backscattering enhancement of electromagnetic waves from two dimensional random rough surfaces with the forward-backward/novel spectral acceleration method," J. Opt. Soc. Am. A **18**, 2518–2525 (2001).
20. C. Macaskill, "Geometric optics and enhanced backscattering from very rough surfaces," J. Opt. Soc. Am. A **8**, 88–96 (1991).
21. K. A. O'Donell and E. R. Mendez, "Experimental study of scattering from characterized random surfaces," J. Opt. Soc. Am. **4**, 1194–1204 (1987).
22. "Observation of depolarization and backscattering enhancement in light scattering from Gaussian random surfaces," Opt. Commun. **61**, 91–95 (1987).
23. I. Simonsen, A. A. Maradudin, and T. A. Leskova, "The scattering of electromagnetic waves from two dimensional random rough penetrable surfaces," Phys. Rev. Lett. (to be published).
24. L. Zhao, K. P. Nielsen, J. K. Lotsberg, E. Marken, J. J. Stamnes, and K. Stamnes, "New versatile setup for goniometric measurements of spectral radiance," Opt. Eng. **45**, 053606 (2006).
25. H. Parviainen and K. Muinonen, "Rough-surface shadowing of self-affine random rough surfaces," J. Quant. Spectrosc. Radiat. Transfer **106**, 398–416 (2007).
26. K. Fu and P. Hsu, "New regime map of the geometric optics approximation for scattering from rough surfaces," J. Quant. Spectrosc. Radiat. Transfer **109**, 180–188 (2008).
27. P. Beckmann and A. Spizzichino, *The Scattering of Electromagnetic Waves from Rough Surfaces* (Pergamon, 1963).
28. J. Jaglarz, R. Duraj, P. Szopa, J. Cisowski, and H. Czternastek, "Investigation of white standards by means of bidirectional reflection distribution function and integrated sphere methods," Opt. Appl. **XXXVI**, 97–103 (2006).
29. H. Noble, W. T. Lam, G. Smith, S. McClain, and R. A. Chipman, "Polarization scattering from a spectralon calibration sample," Proc. SPIE **6682**, 668219, doi:10.1117/12.747483 (2007).